Settling of Dilute and Semidilute Fiber Suspensions at Finite *Re*

J. Salmela
VTT Processes, FIN-40101, Jyväskylä, Finland

D. M. Martinez
Dept. of Chemical and Biological Engineering, University of British Columbia, Vancouver BC, Canada

M. Kataja
Dept. of Physics, FIN 40014 University of Jyväskylä, Finland

DOI 10.1002/aic.11245
Published online June 28, 2007 in Wiley InterScience (www.interscience.wiley.com).

The motion of tracer fibers settling in a suspension made optically transparent using an index-of refraction matching technique is studied as a function of concentration, aspect ratio, fluid viscosity, and fiber length distribution. At $\mathrm{Re} \sim O(1)$*, two different regimes of sedimentation are clearly identified. For small volume fractions we find that fibers settle with their long-axis preferentially in the horizontal state. With increasing volume fraction, fibers settle preferentially with their long-axis aligned in the direction of gravity. These findings are strikingly different than for those conducted with* $\mathrm{Re} \rightarrow 0$ *and qualitatively support the numerical simulations reported by Kuusela et al.*
 AIChE J, 53: 1916–1923, 2007
Keywords: setting/sedimentation, fibers, fluid mechanics

Introduction

The focus of the present work is an experimental study of the motion of settling non-Brownian glass fibers in a Newtonian fluid at $Re \rightarrow O(1)$. Although the settling process is found in a number of industrial and natural settings, there are still many unanswered fundamental questions regarding the mechanism for particle dispersion (mixing) or clumping (flocculation). A part of the motivation for the present investigation stems from an interest in the paper-making process. Under normal processing conditions, these suspensions aggregate naturally into flocs or clumps, which possess measurable strength.[1] Fiber flocculation is a deleterious effect as it creates paper that appears cloudy or grainy when examined in light.

Correspondence concerning this article should be addressed to D. M. Martinez at martinez@chml.ubc.ca.

There are large number of studies found in the literature, which consider sedimentation and particle clumping. In general, studies of settling in Stokes' flow, $Re \leq 1$, focus on understanding the long-range hydrodynamic interactions. Insight into this can be gained by examining the simplest case of the motion of a single isolated fiber settling under Stokes' flow conditions,[2,3] i.e.,

$$\mathbf{v}_{\mathrm{sed}} = \frac{\Delta\rho d^2}{16\mu}\left[\left(\ln 2r + 0.193 + O(\ln 2r)^{-1}\right)\mathbf{g} + \left(\ln 2r - 1.807 + O(\ln 2r)^{-1}\right)(\mathbf{p}\cdot\mathbf{g})\mathbf{p}\right] \quad (1)$$

where $\Delta\rho$ is the difference in density between the fiber ρ and surrounding fluid ρ_{f} ; r is the aspect ratio of the fiber defined by l/d, where d is the diameter of the fiber; μ is the viscosity of the fluid; $\mathbf{g}$ is the acceleration due to gravity; and $\mathbf{p}$ is a unit vector that indicates fiber orientation. Unlike

spheres, fibers can have significant motion perpendicular to gravity with a drift velocity strongly dependent upon its orientation. To illustrate this behaviour, Jayaweera and Mason[4] examined the motion of single particles falling in a large tank with a viscous liquid. At low Re, $Re < 0.01$, these authors report that during descent the cylinders show no preferred orientation; they tended to fall in the same attitude with which they were released.

For cases above this dilute limit, this situation becomes more complex as each individual fiber settles and rotates under the influence of the long-range hydrodynamic disturbances of the other settling particles. This leads to inhomogeneous settling rates and local floc formation. This behavior has been observed by Kumar and Ramarao.[5] They reported the existence of flocs for monodisperse glass fibers under dilute conditions. They also noted that as the fiber concentration increased, the number of flocs increased and caused greater hindrance effects. To help understand this behaviour, Herzhaft et al.[6,7] visualized the motion of marked glass fibers, in a suspension of unmarked fibers made optically transparent by matching the index-of-refraction. By doing so, they were able to measure both the velocity and orientation of a particle. They found that in the dilute regime, the ensemble-averaged settling velocity actually increased with concentration and at certain concentrations the velocity may exceed that of an isolated particle. They also observed that under these conditions most of the fibers were aligned in the direction of gravity and occasionally "flipped" during descent. In the semidilute regime, however, the settling velocity decreased monotonically following the phenomenological Richardson–Zaki correlation.[8]

There are only a few theories and simulations available in the literature, which attempt to describe this process.[3,9,10] In general these works were conducted in the limit of $Re \rightarrow 0$, using slender body theory, and suggest that the settling suspension should segregate into particle clumps. Koch and Shaqfeh[9] were the first to describe an instability mechanism that leads to floc formation. They advance an argument that a "test" fiber in the velocity field far from a sedimenting single fiber tends to orient its main axis such that the relative velocity of the two particles become negative. Thus, the particles will tend to form clusters until near-field effects or contact forces intervene. Mackaplow and Shaqfeh[3] present two different numerical results using (i) Monte-Carlo simulations of static fiber assemblies and (ii) point-particle approximations for the dynamic case. They observed fiber clustering and velocities greater than that of an isolated particle. In more recent work Butler and Shaqfeh[10] simulated the motion of swarms of particles and observed fiber clustering. Their simulations were in good agreement with experimental results of Herzhaft et al.,[6] and Herzhaft and Guazzelli.[7]

It has been shown that, unlike in the Stokes' regime, at Reynolds numbers $Re \sim O(1)$ isolated nonspherical particles tend to exhibit preferential orientation during settling.[4,11,12] In particular, the torque induced on thin cylinders causes the body to rotate into a stable position with its symmetry axis aligned horizontally. Furthermore, Feng et al.[11] show that isolated particles migrate towards the center of the channel because of wall effects. In perhaps the most relevant work for the case considered here, Kuusela et al.[13,14] have simulated sedimentation at $Re \sim O(1)$ and confirm that in the dilute limit spheroids prefer the horizontal orientation. When the volume fraction increases, these authors demonstrate that spheroids begin to align themselves parallel with gravity. This is an important difference when compared with the sedimentation of fibers under Stokes' conditions.

To summarize the existing literature, it is well established through both experimental and simulation results that fibers tend to clump, and orient themselves in the vertical direction when settling with $Re \rightarrow 0$. In the dilute regime, fiber clumping results in settling rates faster than that of an isolated particle. At larger Re, i.e., $Re \sim O(1)$, there is evidence generated from numerical simulations indicating that under dilute conditions settling particles assume a horizontal orientation; under semidilute conditions fibers settle preferentially with a vertical orientation. These findings have yet to be confirmed experimentally and it is our intention in this work to do so.

In this work we extend the results reported by Herzhaft and Guazzelli by examining the motion of settling glass fibers over a wider range of Reynolds numbers ($3 \times 10^{-4} \leq Re \leq 9$) and investigate the effect of volume fraction, aspect ratio, and fiber length distribution (mono-and bidispersed suspensions). Of special interest is the range $Re \sim O(1)$ that is relevant, e.g., paper-making applications.[15] In particular, we intend to confirm two aspects of Kuusela's numerical simulations[14] in this Reynolds number regime, namely that (i) in the dilute limit spheroids tend to adopt a vertical orientation, and (ii) with increasing concentration spheroids prefer the horizontal state.

Experimental Techniques

Our apparatus resembles the experimental systems used by Nicholai et al.[16] for spheres and Herzhaft and Guazzelli[7] for rods. What sets our system apart from these previous studies is that we acquire the full three-dimensional motion of the particles, i.e., position, orientation, and velocity in both the (x, z) and (y, z) planes. This modification was necessary as we study bidispersed suspensions that have two different fiber length fractions. The length of each particle can only be determined, using a 3D reconstruction method.

The experiments were performed in a square cross-sectional Plexiglas® cell (100×100 mm^2) with $\sim$2.0 l of suspension. Two sets of cylindrical glass fibers (www.mosci.com) of dimensions 2.3×0.1 mm^2 and 5×0.1 mm^2 were employed. The glass fibers had a density of $\sim$2250 kg/m^3. The index of refraction of these fibers was measured commercially and found to be 1.4719 ($\pm$0.0005) (www.integrextesting.com). Approximately 2% of the fibers in each suspension were silvered using Tollen's solution, a mixture of 5 ml of 0.1 M $AgNO_3$ with $\sim$10 μl (5 drops) of 0.4 M NaOH. Before silvering, the fibers were washed in detergent, rinsed in alcohol and then in distilled water. After silvering the fibers were again washed in a similar manner to remove any loosely adsorbed $AgNO_3$. Finally the tracer fibers were inspected, using a microscope, and all of the damaged fibers were removed.

A listing of the experimental systems studied is shown in Table 1. In Series 1 and 2, we measure the motion and orientation of monodispersed suspensions as a function of Re near the dilute limit. The Newtonian fluids used in these series were created by mixtures of glycerine and water. In Series

Table 1. The Experimental Conditions Studied

Series	Fluid Properties μ, Pa s, 23°C	Aspect Ratio r	Concentration ϕ, % vol	Re
1	0.015–1.12	23	3.7×10^{-4}	0.0004–2
2	0.015–1.12	50	3.7×10^{-4}	0.001–9
3	0.036	23	0.01–0.4	0.07
4	0.036	50	0.01–0.4	0.23
5	0.036	Bidispersed*	0.07–0.5	$0.01 \leq Re \leq 0.23^{\dagger}$

*Equal mixture (by mass) of each fiber type.
†A range for Re is given here as we do not have one characteristic fiber length.

3–5, we investigate the effect of concentration. In this case the fluid used was a mixture of Drakeol 35 and Penrico 6970 mineral oils ($\rho = 858$ kg/m^3) (Polygon). In Series 5, the suspension was composed of an equal mass of both fiber types; this implies that the number density of each component is different. A minimum of nine concentration or viscosity levels were performed in each series. At each experimental point, three separate measurements were conducted.

The experimental procedure was composed of a period of mixing followed by a period of settling. The particles were forced into suspension by agitating the fluid with an impeller. The impeller speed was kept low to prevent breakage of the glass fibers. The impeller was then removed from the tank and a waiting period of 15–20 s was required to ensure that all impeller-induced motion had subsided. Imaging commenced at this point. For each series of experiments, the imaging rate was adjusted so that the mean fiber displacement between images and the number of acquired images were constant. By this the total fiber displacement during image acquisition sequence was kept constant and independent of the mean sedimentation velocity. It should be noted that the testing proceeded in a temperature controlled room and no convection currents resulting from heating from the lamps were observed.

Our visualization system consisted of a progressive scan Basler A201b monochrome CCD camera (10 bit grey scale and 1008 × 1018 pixel spatial resolution with a maximum framing rate of 30 frames per second), mounted with an F-mount Micro-NIKKOR 105-mm lens. A system of first surface mirrors were employed so that two perpendicular faces of the sedimentation jar could be imaged simultaneously using only one camera (see Figure 1). With the optical setup described the imaged volume is 60 × 60 × 70 mm^3 (length × width × elevation). Since the width of the sedimentation jar is 100 mm there is a 20-mm gap between jar wall and imaged volume. This ensures that walls have no effect on our results. The volume imaged is also far from the bottom of the sedimentation jar (50 mm) and from the air–oil surface (80 mm).

For particle tracking, the lens aperture and focus, backlight intensity and camera exposure time were chosen so that the whole imaged volume was within the depth of field of the lens. The sedimentation jar was transilluminated, using Schott-Fostec fiber optic dual backlight. The images were captured and saved, using a Matrox MeteorII digital frame grabber. Fiber sedimentation velocity is calculated using an in-house fiber tracking algorithm and consists of the following subroutines:

(1) *Image enhancement:* Performed using the method outlined by Kellomaki et al.[17] This method allows for corrections due to unevenness in the illumination field and removes all static grey-scale variations (e.g., dirt).

(2) *Particle identification:* Performed using the built-in edge detection algorithm (gradient method) in MATLAB. This routine includes morphological operations to exclude all moving elements, which do not match the dimensions of the tracer particles.

(3) *Velocimetry:* Performed by measuring the vertical, horizontal, and orientational displacements of the fibers between sequential binary images. We do so using a cross-correlation with a window, which has been specially selected to have only one matched particle. Special care was required for cases, in which the fibers appeared as crossed. From these images, the position, velocity, and orientation of each tracer fiber could be determined.

(4) *3D Reconstruction:* Performed by searching both images to find the corresponding fibers with identical velocities and elevations.

(5) *Particle identification:* Performed as we used bidispersed suspensions in Series 5. In this case, once the 3D reconstruction was completed, the length of each fiber was determined and then sorted according to size.

Results and Discussion

Before proceeding to the main findings of this section, it is instructive to ascertain whether steady state has indeed been achieved by the time of commencing the measurement. To this end, we plot the mean drift velocity $\langle V_{\perp} \rangle$ and settling velocity $\langle V_{\parallel} \rangle$ and velocity functions $\langle V \backslash \mathrm{perp}' \rangle$ and $\langle V'_{\parallel} \rangle$ as a function of time, see Figure 2. At each time step, between 30 and 120 instantaneous velocity measurements were used in the ensemble-average. The error bar represents the 95% confidence interval for this mean. It should be noted that the results have been made dimensionless by scaling the ensemble-average velocity with the velocity of an isolated particle settling in the vertical orientation ($V^i_{\parallel}$). This value was determined experimentally and for the monodispersed case it

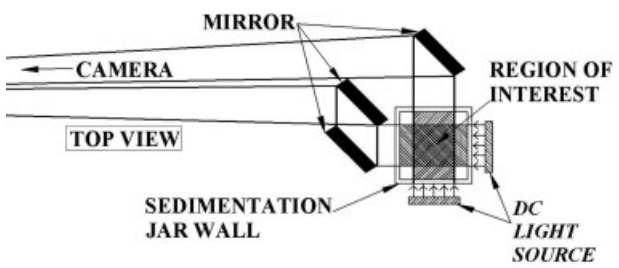

Figure 1. Illustration of the experimental set-up.

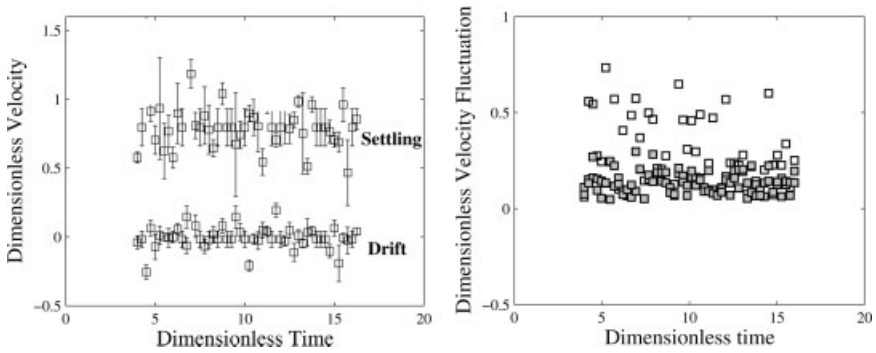

Figure 2. On the left panel the dimensionless mean drift $\langle V_\perp \rangle^*$ and settling $\langle V_\parallel \rangle^*$ velocities versus dimensionless time t^* for $\phi = 1 \times 10^{-3}$% and fiber aspect ratio $r = 50$ ($Re = 0.23$).

The uncertainty in the data is reported at the 95% confidence interval (open symbols for settling velocity fluctuations and hatched symbols for drift velocity fluctuations). On the right panel dimensionless velocity fluctuations in the settling velocity versus dimensionless time is shown for the same data.

equals the estimate given by Eq. 1. The Reynolds number quoted in this work are based upon the length of the fiber and $\langle V_\parallel \rangle$. Time has been scaled using $l/V^i_\parallel$. All starred variables (*) from this point forward represent dimensionless quantities. In this example, $t^* = 0$ represents the point in time where the mixer was removed from the sedimentation jar. We find that at this point there was an initial swirl induced by the impeller that dampened quickly. Imaging commenced at $t^* > 4$. In the region in time sampled, we conclude that steady state was achieved as the drift velocity fluctuated about zero and that there were no statistical differences between the means of $\langle V_\parallel \rangle^*$ for each time step recorded. We found this for all cases tested. A similar conclusion has been drawn for the velocity fluctuations. These results differ strongly from previous results at $Re \to 0$ by Herzhaft et al.,[6] and Herzhaft and Guazzelli,[7] who find that steady state was achieved at a Stokes' time of 50–200. As a result the apparent steady state, for which we present evidence for, may really only be a transient plateau or that there may be a steady behavior of some parameters and not others. To illustrate this point we estimate, roughly, the angular velocity $\dot{\theta}$ of a settling isolated particle at $Re \sim 1$. To do so we use the expressions developed by Khayat and Cox, as summarized by Shin et al.,[18] to estimate the force and torque acting on the particle. For an isolated particle in an unbounded fluid whose angle θ measured relative to the horizontal is small, the approach of the angle to zero is estimated to be

$$\frac{d\dot{\theta}}{dt} = -\frac{5Re\theta}{8\ln r} \tag{2}$$

This indicates that under some experimental conditions steady state may not be reached in this variable. In any case, imaging proceeded in a period in which the settling, drift, and fluctuating components appeared essentially steady.

The histograms of the velocities for each time step were then superimposed and found to be smooth and clustered around a definite value. Like Herzhaft and Guazzelli,[7] we find that the velocity distribution was clustered near zero (see the left panel of Figure 3). For each concentration tested, the mean velocity was determined from the ensemble-average of all time steps. This is shown in the right panel of Figure 3. The first observation that can be made from this

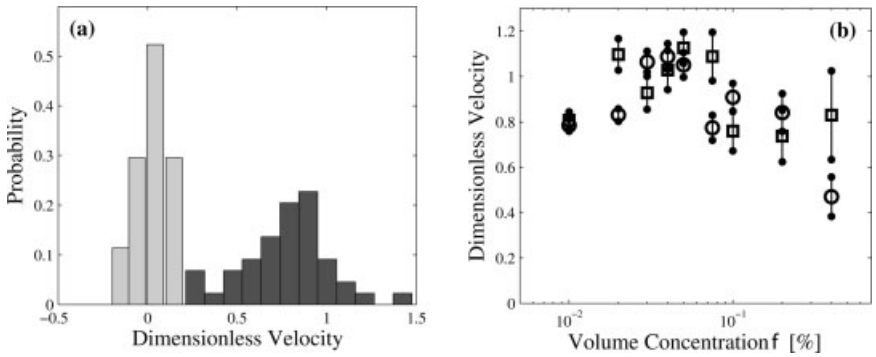

Figure 3. On the left panel an example of velocity distribution histogram ($r = 23$, $c = 0.001$%).

The dark bars represent the settling velocity, while the grey bars represent the drift velocity. On the right panel the dimensionless mean settling velocity $\langle V_\parallel \rangle^*$ versus volume concentration ϕ, for fiber aspect ratio $r = 50$ (□) and $r = 23$ (○). The uncertainty in the estimate is reported as the 95% confidence interval ($Re_{r=23} = 0.07$ and $Re_{r=50} = 0.23$).

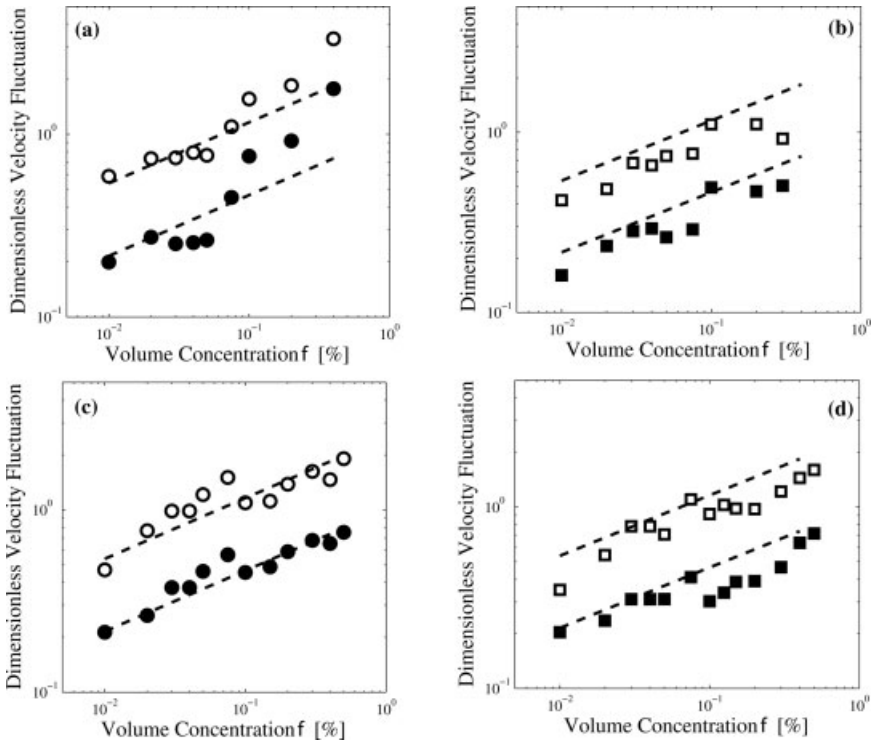

Figure 4. The dimensionless mean settling $\sigma_{\|}/\langle V_{\|}\rangle$ and drift $\sigma_{\perp}/\langle V_{\|}\rangle$ velocity fluctuations versus volume concentrations ϕ for: (a) $r = 23$, $Re = 0.07$ (Series 3); (b) $r = 50$, $Re = 0.23$ (Series 4); (c) $r = 23$ (Series 5); and (d) $r = 50$ (Series 5).

The unfilled symbols represent the settling fluctuations whilst the filled ones represent drift fluctuations. The hatched lines (-) indicate $\phi^{1/3}$ behavior.

figure is that a maximum settling velocity occurs at $\phi \approx 0.05\%$ for both types of fibers tested. The average velocity at this point exceeds the settling velocity of an isolated particle. This behavior has also been reported by other researchers.[6,7,14] In these studies, however, the concentration where the maximum is observed is much higher than that reported in our work. In addition to the ensemble average, we examined the spread in the velocity histograms and represent this as the standard deviation, σ, see Figure 4. We find that that both the drift and settling velocity fluctuations are approximately proportional to $\phi^{1/3}$. Next, we examine the ratio of the velocity fluctuations in the horizontal and settling direction, i.e., $\sigma_{\|}/\sigma_{\perp}$, and define this measure as the fluctuation anisotropy, see Figure 5. Our results indicate that the fluctuation anisotropy varies in the range of 1.5–3. For the monodispersed case, the fluctuation decreases over the concentration range tested, whereas it is approximately constant for the bidispersed case. Finally, we examined the settling velocity of the particles as a function of orientation, i.e., $\langle V_{\|}(\theta)\rangle^*$. The superimposed data were sorted according to its orienta-

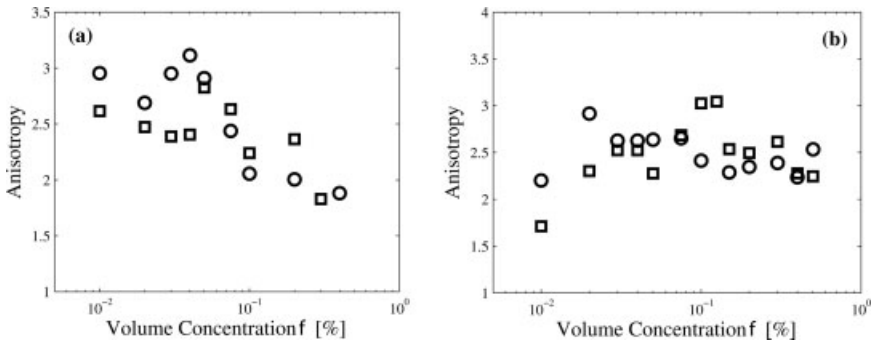

Figure 5. The anisotropy in the velocity fluctuations $\sigma_{\|}/\sigma_{\perp}$ versus volume concentration ϕ for: (a) the monodispersed cases (Series 3 $Re = 0.07$ and Series 4 $Re = 0.23$); and (b) the bidispersed case (Series 5).

The cases with fibers with an aspect ratio of $r = 23$ are shown as circles (○) and fibers with an aspect ratio $r = 50$ are shown as squares (□).

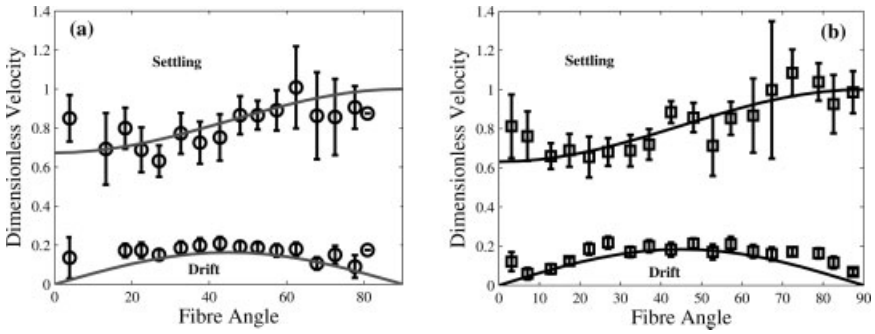

Figure 6. The dimensionless mean drift $\langle V_\perp \rangle^*$ and settling $\langle V_\parallel \rangle^*$ velocities versus fiber angle θ measured relative to the horizontal for $\phi = 0.01\%$.

The figure on the left (a) represents experimental Series 3 ($Re = 0.07$), while (b) represents experimental Series 4 ($Re = 0.23$). The uncertainty in the estimate is reported as the 95% confidence interval. The variations in confidence levels are due to different number of fibers found in each angle bin.

tion and the velocity of all particles at each angle was ensemble-averaged. The results are shown in Figure 6 for the case $\phi = 0.01\%$. Included in this figure is a solid line representing Eq. 1. This result may be interpreted as an indication that (i) fiber–fiber interactions are small at this relatively low concentration, (ii) steady-state has been achieved during imaging, and (iii) our tracking algorithm is producing correct results. At higher concentrations the agreement between the data and Eq. 1 diminishes.

We now turn to the main findings of this work, namely the orientation distribution. As with the velocity measurements, the data from each time step were superimposed to create a probability distribution for fiber orientation. Following Herzhaft and Guazzelli and Kuusela et al.,[14] we characterize these distributions using an "order parameter" Ψ defined as $\Psi = \langle 2\cos^2 \theta - 1 \rangle$, where θ is the orientation angle measured from horizontal direction. To illustrate the behavior of this function, $\Psi = -1$ implies that all of the fibers are oriented in the direction of gravity. If $\Psi = 1$, the fibers are aligned horizontally; $\Psi = 0$ represents an isotropic distribution. The results in the dilute limit are shown in Figure 7. The first observation that can be made from this figure is that there are three distinct regions namely (a) $Re < 10^{-2}$, (b) $10^{-2} < Re < 0.5$, and (c) $Re > 0.5$. The first region, $Re < 10^{-2}$, has been documented by Jayaweera and Mason,[4] and it is well established that in the dilute limit fibers tend to fall in the same attitude with which they were released. As a result, the distributions reported in this region reflect the orientation state of the suspension at the cessation of mixing. In the second region, $10^{-2} < Re < 0.5$, we find that the order parameter is constant and clustered around a value of $\sim$0.3. In the third region, i.e., $Re > 0.5$, the fibers preferentially align themselves with their axes aligned in the vertical direction. Our results in this region are qualitatively similar to those reported by Jianzhong et al.,[12] and Kuusela et al.[14]

Above this dilute limit, the effect of concentration on Ψ is shown in Figure 8. For Series 3 and 5, shown as Figures 8a,c, the results indicate that the suspension was preferentially oriented in the horizontal state at low concentrations and then adopted an increasing proportion of fibers in the vertical state as concentration increased. These results tend to qualitatively confirm the numerical results of Kuusela et al.[14] A more rigorous comparison can not be made at this point as there are differences between the Re number and volume fraction in this study and our experimental work. We also compared our findings with that reported by Herzhaft and Guazzelli[7] for the case most similar to our work, i.e., $r = 20$. This result is shown as black circle in Figure 8. Although the value of the order parameter is quite similar for these two studies, our observations of the settling fibers are different. We found that fibers rotate slowly during the descent. Instead, we did not observe particular "flipping" motion.

It is difficult to ascertain if the result reported in Figure 8b displays the same trend as that in Figures 8a,c. What is evident here is that there are two clusters of data. The first cluster is at the lower end of the concentrations measured and is centered around $\Psi \sim 0.15$. The second cluster of data, at the higher end of the concentrations measured, is clustered around $\Psi \sim -0.05$. The two clusters are statistically different from each other at the 95% confidence level. What is

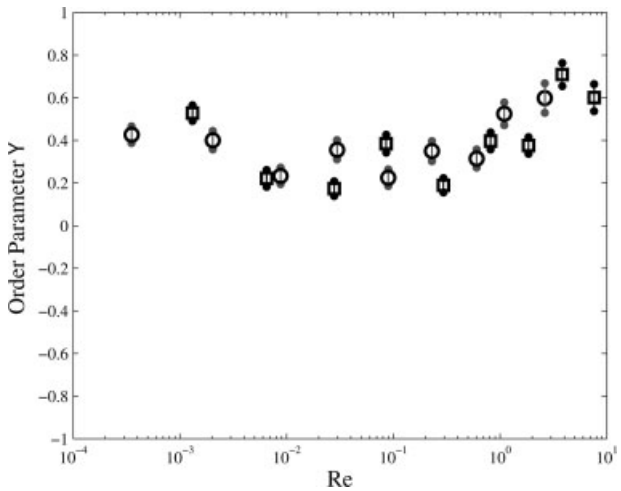

Figure 7. The effect of Reynolds number on the average fiber orientation Ψ in the dilute limit.

In this case the concentration of the suspension was $\phi = 3.7 \times 10^{-4}\%$ vol.

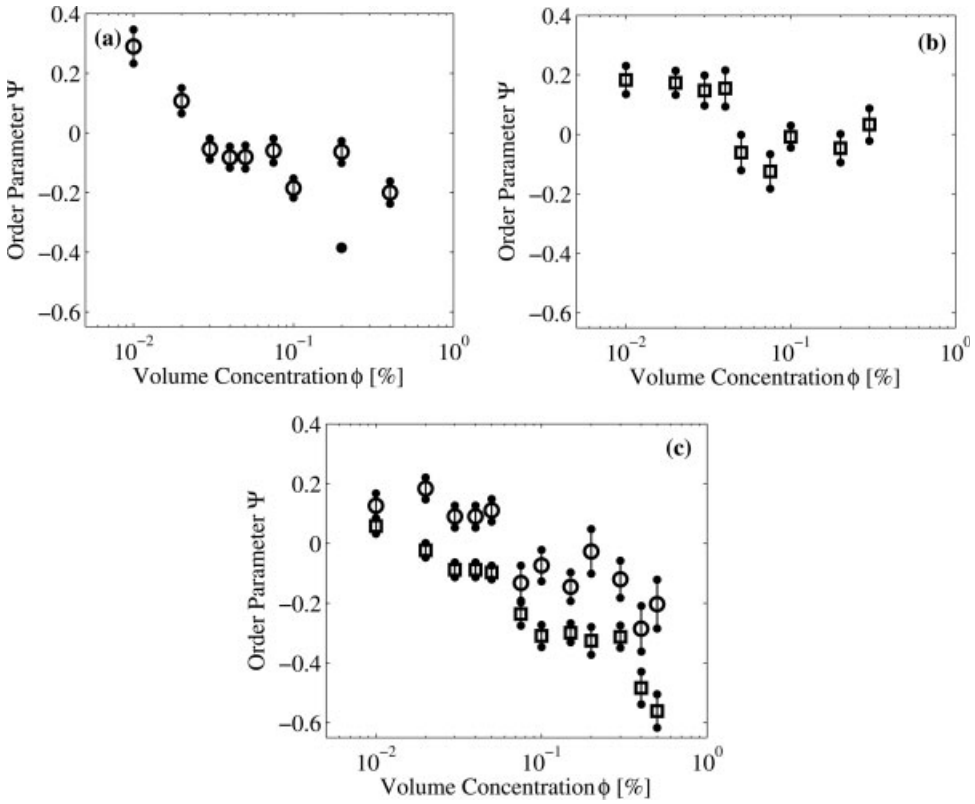

Figure 8. The order parameter Ψ versus volume concentration ϕ for: (a) Series 3 ($r = 23$, $Re = 0.07$); (b) Series 4 (r equals; 50, $Re = 0.23$); and (c) Series 5.

The ● in (a) represents a result by Herzhaft and Guazzelli[7] for $r = 20$, $Re < 0.001$.

clear from the literature is that for settling spheres the velocity fluctuations are very sensitive to the ratio of vessel size to particle size. There is no reason to believe that this would not occur with rigid rods also. In this figure, this ratio has not been held constant and perhaps represents the reason why the trend in order parameter is not as clearly defined as in the other two cases reported.

Summary and Conclusions

In this work we measured the motion of individual tracer particles in settling non-Brownian glass fiber suspensions with $Re \rightarrow 1$. We employed a three-dimensional tracking system whereby the full motion of the particles could be captured. We show that the steady-state settling velocity has a maximum at small volume fractions. This maximum which was found to exceed the velocity of an isolated particle has been previously attributed to cluster formation. Our results, however, reveal that this is accompanied by a change in average fiber orientation namely, (i) in the dilute limit the fibers preferentially orient themselves in the horizontal position with $Re > 0.5$ and (ii) with increasing concentration, the $r = 23$ and bidispersed suspension fiber adopt a vertical orientation. We believe that this results stems from increasing fiber–fiber collisions destabilizing the horizontal state. Finally we find that these observations qualitatively support the numerical simulations of Kuusela et al.[14]

Acknowledgments

Financial support from the Natural Sciences and Engineering Research Council of Canada and the Advanced Papermaking Initiative is gratefully acknowledged.

Literature Cited

1. Mason SG. Fiber motion and flocculation. *Pulp Pap Mag Can*. 1954;55:96–102.
2. Batchelor GK. Sedimentation in a dilute dispersion of spheres. *J Fluid Mech*. 1972;123:245–268.
3. Mackaplow MB, Shaqfeh ESG. A numerical study of the sedimentation of fiber suspensions. *J Fluid Mech*. 1998;376:149–182.
4. Jayaweera KOLF, Mason BJ. The behaviour of freely falling cylinders and cones in a viscous fluid. *J Fluid Mech*. 1965;22:709–720.
5. Kumar P, Ramarao BV. Enhancement of the sedimentation rates of fibrous suspensions. *Chem Eng Commun*. 1991;108:381–401.
6. Herzhaft B, Guazzelli E, Mackaplow MB, Shaqfeh ESG. Experimental investigation of the sedimentation of dilute fiber suspension. *Phys Rev Lett*. 1996;77;290–293.
7. Herzhaft B, Guazzelli E. Experimental study of the sedimentation of dilute and semi-dilute suspensions of fibers. *J Fluid Mech*. 1999;384:133–158.
8. Richardson JF, Zaki WN. Sedimentation and Fluidisation: Part 1. *Trans Inst Chem Eng*. 1954;35:32.
9. Koch DL, Shaqfeh ESG. The instability of a dispersion of settling spheroids. *J Fluid Mech*. 1989;224:275–303.
10. Butler JE, Shaqfeh ESG. Dynamic simulations of the inhomogeneous sedimentation of rigid fibers. *J Fluid Mech*. 1998;468:205–237.
11. Feng J, Hu HH, Joseph DD. Direct simulation of initial value problems for the motion of solid bodies in a Newtonian fluid, Part 1: Sedimentation. *J Fluid Mech*. 1998;261:95–134.

12. Jianzhong L, Xing S, Zhenjiang Y. Effects of the aspect ratio on the sedimentation of a fiber in Newtonian fluids. *J Aerosol Sci*. 2003;34:909–921.
13. Kuusela E, Hoefler K, Schwarzer S. Computation of particle settling speed and orientation distribution in suspensions of prolate spheroids. *J Eng Math*. 2001;41:221–235.
14. Kuusela E, Lahtinen JM, Ala-Nissila T. Collective effects in settling spheroids under steady-state sedimentation. *Phys Rev Lett*. 2003; 90:094502–1.
15. Marton R, Robie JD. Characterization of mechanical pulps by a settling technique. *Tappi J*. 1969;22:2400–2406.
16. Nicholai H, Herzhaft B, Hinch EJ, Oger L, Guazzelli E. Particle velocity fluctuations and hydrodynamic self-diffusion of sedimenting non-Brownian spheres. *Phys Fluids*. 2003;7:12–23.
17. Kellomäki M, Karema H, Kataja M. Fiber flocculation measurement in pipe flow by digital image analysis. In: *Proceedings of TAPPI International Paper Physics Conference*, San Diego, Tappi Press (Atlanta) 1999:461–463.
18. Shin M, Koch DL, Subramanian G. A pseudospectral method to evaluate the fluid velocity produced by an array of translating cylinders. *Phys Fluids*. 2006;18:063301–1.

Manuscript received Aug. 14, 2006, and revision received May 22, 2007.